RSC Advances

PAPER

View Article Online
View Journal | View Issue

Cite this: *RSC Adv.*, 2025, **15**, 48072

A polyelectrolyte stabilizer cooperating with sodium silicate to stabilize surplus soils from engineering projects to establish dual-crosslinking flowable stabilized soil

Haiyang Zhang,[a] Dengliang He,*[a] Shishan Xue,*[a] Shuxin Liu,[a] Mengyong Ran[b] and Yi Liu[b]

With the rapid development of modern society, the increasing construction of various large-scale infrastructure projects leads to the substantial generation of engineering surplus soils, greatly increasing the cost due to the pollution they cause in the surroundings. In this work, three kinds of anionic polyelectrolyte soil stabilizers [P(AA-*co*-AM), L-PAA, and H-PAA] were synthesized, which coordinated with sodium silicate (SS) to fabricate flowable stabilized soil (FSS), exhibiting an outstanding original fluidity of 202.33 mm, significantly exceeding the 180 mm threshold required for pumpable FSS. Meanwhile, the soil matrix stabilized by L-PAA and SS displayed the highest 28 day compressive strength of 6.25 MPa. This work presents a novel strategy for rapidly stabilizing engineering surplus soils, thereby significantly reducing the disposal cost, which is important in the field of construction engineering.

Received 15th July 2025
Accepted 18th November 2025

DOI: 10.1039/d5ra04933d

rsc.li/rsc-advances

1 Introduction

The rapid expansion of urban infrastructure, encompassing transportation networks, built environments, underground utilities, and coastal developments, generates substantial quantities of construction-related surplus soils. Appropriate treatment of these engineering surplus soils is imperative to mitigate potential environmental contamination, avoid resource depletion, and ensure compliance with environmental regulations. Traditional disposal practices for engineering surplus soils typically involve off-site landfilling, which involves significant logistical challenges, including substantial transportation expenses, land consumption and long-term geotechnical risks such as ground subsidence. Recently, *in situ* treatment and resource recovery of engineering surplus soils have gained prominence as sustainable geotechnical solutions. However, the intrinsic properties of soil, including unconfined compressive strength, shear stability, and hydraulic conductivity, do not satisfy the requirements of construction applications or environmental rehabilitation. The exploitation of a novel approach to solidify or stabilize these soils is in high demand in the field of construction engineering.[1–3]

Many materials have been utilized to stabilize these soils, including cementitious (*e.g.* Portland cement, calcium oxide, coal fly ash, and ground granulated blast furnace slag, *etc.*)[4–7] and organic materials (*e.g.* vinyl acetate-ethylene, polyacrylate, xanthan gum, *etc.*).[8–11] Cementitious materials promote the establishment of calcium silicate hydrate (C–S–H) gels and other cementitious phases through two pozzolanic reactions and hydration processes to form cementitious gels to densify soil matrices to create three-dimensional cementation networks.[12–15] Organic materials enhance mechanical properties through physical adsorption *via* van der Waals forces and hydrogen bonding at particle interfaces,[16] chemical bonding through covalent/ionic interactions with soil minerals,[17] and three-dimensional networks formed by *in situ* polymerization.

Hou *et al.*[4] systematically evaluated the stabilization performance of sodium silicate-activated slag/fly ash composites on soft clay soils. Through comprehensive laboratory testing, the researchers identified an optimal stabilizer formulation comprising 3 wt% sodium silicate activator and 5 wt% fly ash additive, which produced stabilized soils with a 28 day unconfined compressive strength (UCS) of 0.85 MPa. Abdelbaset *et al.*[5] developed an innovative stabilization system for kaolinitic soils using fly ash-lime blends. Experimental results demonstrated that the optimal composition containing 15 wt% class F fly ash and 3 wt% hydrated lime achieved a 28 day UCS of 0.63 MPa. Eshghi *et al.*[6] developed an innovative stabilization strategy for fine-grained clay soils by synergistically combining natural zeolite (5 wt%) with nano-scale magnetite (1 wt% Fe_3O_4). The composite stabilizer system demonstrated remarkable performance, yielding a 28 day UCS of 0.45 MPa.

[a]*Chemistry and Material Engineering School, Mianyang Teachers' College, Mianxing West Road No. 166, Mianyang City, Sichuan Province, 621000, China. E-mail: 449011902@qq.com; xueshishancarol@163.com*

[b]*Chengdu Yongtuo Building Materials Co., Ltd, Wen'an Community, Hong'an Town, Longquanyi District, Chengdu City, Sichuan Province, 610108, China*

The organic materials utilized for stabilizing soils have also been widely reported. For example, Luan *et al.*[8] demonstrated that a vinyl acetate-ethylene (VAE) copolymer emulsion could effectively stabilize subgrade clay through interfacial polymerization. At optimal dosage levels (0.025–0.03 wt%), the treated soil achieved a 28 day UCS of 1.30 MPa. Wang *et al.*[9] systematically investigated the polyacrylate (PA)-based stabilization of granite residual soil, revealing that a 2 wt% PA dosage enhanced the mechanical properties. Liu *et al.*[10] evaluated the stabilization performance of an ethylene-vinyl acetate (EVA) copolymer emulsion on expansive clay. The 1 wt% EVA-treated specimens exhibited a 28 day UCS of 0.35 MPa. Ayeldeen *et al.*[11] systematically evaluated the stabilization of collapsible soils using biopolymers, demonstrating that xanthan gum at a 2% concentration (by dry soil weight) significantly enhanced the soil mechanical properties after 7 day curing. Soltani *et al.*[18] conducted a comprehensive investigation on the cyclic swell-shrink behavior of highly expansive soil treated with anionic polyacrylamide (PAM, $M_w \approx 8 \times 10^6$ Da). The results indicated that 0.2 g L^{-1} PAM could be identified as the optimal dosage for minimizing soil heave and shrinkage induced by swelling-shrinkage cycles.

These works verified the capacity of cementitious and organic materials for stabilizing soils. However, they displayed weaknesses, like compromised effectiveness in high-moisture-content soils and poor water resistance, respectively. The integrated application of organic and inorganic stabilizers can complement their respective advantages, holding significant importance for engineering soil stabilization and the enhancement of mechanical properties in stabilized soils. Moayed *et al.*[19] developed a sustainable stabilization system for kaolin clay through synergistic application of industrial byproducts and natural fibers. The optimal composition containing 6% lime kiln dust, 10% nano-silica, and 0.5% hemp fibers achieved a 28 day UCS of 1.98 MPa. Baghini *et al.*[20] developed a high-performance stabilization system through the synergistic combination of carboxylated styrene-butadiene rubber (SBR) emulsion and Portland cement. The optimized formulation containing 4 wt% cement and 8 wt% SBR exhibited an exceptional 28 day UCS of 11 MPa. Jarjusey *et al.*[21] pioneered a sustainable stabilization approach utilizing agricultural byproducts, developing a ternary bio-composite comprising banana leaf powder, orange peel pectin, and class F fly ash. The optimized formulation (5% BLP + 3% OPP + 12% fly ash by soil weight) demonstrated a 28 day UCS of 1.50 MPa. Wang *et al.*[22] systematically investigated the synergistic stabilization of organic dredged sludge using Portland cement activated by sodium persulfate ($Na_2S_2O_8$). The incorporation of 6 wt% SP resulted in a remarkable 28 day UCS of 2.23 MPa. These materials exhibited outstanding performance in high-water-content soils, contaminated soils, and special geotechnical engineering applications, making them a current research focus in soil stabilization technology.

However, these soil stabilization technologies primarily focus on the mechanical properties of the stabilized mass, while overlooking constructability in complex scenarios such as ground improvement, tunnel backfilling, pipeline embedding, and slope stabilization. These applications require the high fluidity of soil slurry to achieve pumpable construction. In the evolution from traditional stabilization methods, FSS has emerged as a novel engineering material. It is produced by mixing soil, stabilizers, water, and additives to form a highly fluid slurry (initially mortar-like, self-levelling, and suitable for confined or complex spaces). After stabilizing, it yields a solidified mass with controllable strength and low shrinkage. FSS integrates the strengths of traditional soil improvement techniques and modern materials science, demonstrating broad application potential in engineering fields such as ground improvement, tunnel backfilling, pipeline embedding, and slope stabilization.

Here, we harnessed the synergistic properties of organic and inorganic materials to engineer a novel composite FSS to effectively treat construction-related surplus soils. Three kinds of anionic polyelectrolyte soil stabilizers were synthesized *via* free-radical polymerization using acrylic acid and acrylamide as monomers, ammonium persulfate as the initiator, and isopropanol as the regulator. Sodium silicate (SS) was subsequently incorporated as an inorganic reinforcer to enhance the properties through the establishment of a dual-crosslinking network (Scheme 1). The organic–inorganic composite soil mass achieved a peak 28 day compressive strength of 6.25 MPa. These findings have important implications for the development of novel organic soil stabilizers on surplus soils, and practical engineering applications including ground reinforcement, tunnel backfill operations, pipeline embedding, and slope stabilization systems.

2 Experimental

We report in detail the raw materials, preparation and characterization procedure in this section.

2.1 Materials

Acrylic acid (AA, 99%) was purchased from Shanghai Macklin Biochemical Technology Co., Ltd Acrylamide (AM, 98%) was obtained from Tianjin Comio Chemical Reagent Co., Ltd (China). Ammonium persulfate (AR, 98%) was obtained from Tianjin Jindong Tianzheng Fine Chemical Reagent Factory (China). Isopropanol (99%) was obtained from Chengdu Jinshan Chemical Reagent Co., Ltd (China). Powdered instant sodium silicate (SS, 18% Na (as Na_2O), 60% Si (as SiO_2)) was supplied by Shanghai Merrier Chemical Technology Co., Ltd (China). Engineering surplus soils were provided by Chengdu Yongtuo Zhonghe Technology Co., Ltd.

2.2 Synthesis of anionic polyelectrolyte stabilizer

The specific parameters of the synthesized organic stabilizer and the corresponding labels are shown in Table S1. Acrylic acid and acrylamide monomers (a certain proportion) were dissolved in 125 mL of deionized water under constant stirring in a three-neck round-bottom flask. Subsequently, a measured amount of isopropanol was added to the aqueous solution, and the mixture was vigorously stirred until a completely homogeneous

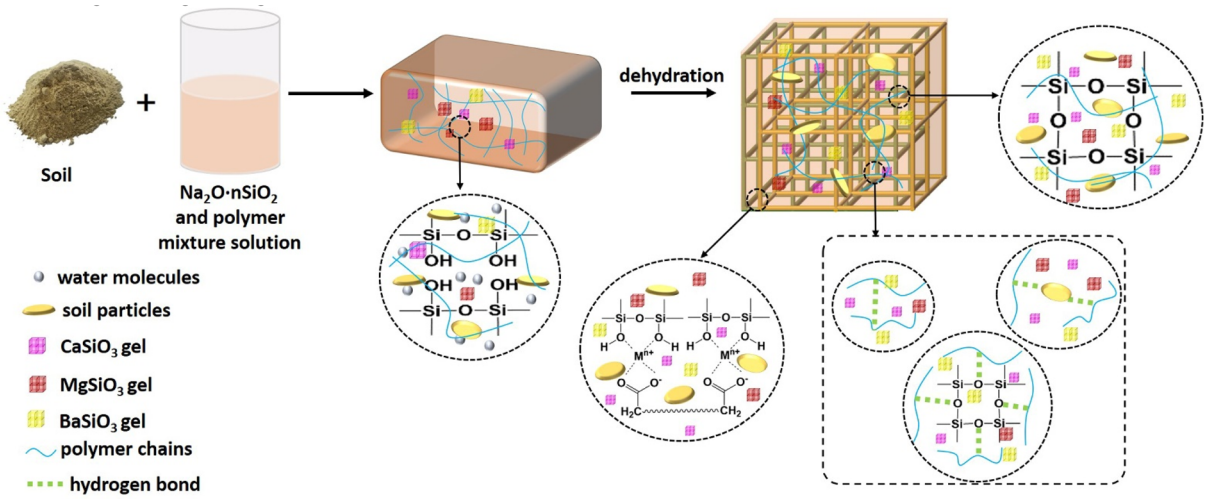

Scheme 1 An illustration of the stabilization mechanism of soil mass stabilized by synthesized polymers and SS.

solution A was obtained. A precisely measured quantity of ammonium persulfate initiator was dissolved in 20 mL of deionized water to prepare initiator solution B. Solution A was degassed with nitrogen for 5 min to remove oxygen. Then, initiator solution B was dropwise added into solution A over a 15-minute period. The reaction mixture was heated to 94 °C under reflux condensation and maintained for 60 min to complete the polymerization. Finally, the resulting viscous polymer solution was cooled to ambient temperature and transferred to airtight amber glass bottles.

2.3 Preparation of flowable stabilized soil

The engineering soil was first pulverized using a planetary ball mill operating at 400 rpm with a 3 : 1 ball-to-powder ratio for 2 h. The resulting material was sieved through a 0.5 mm mesh and subsequently dried in an oven at 90 °C for 3 h. A precisely weighed amount of the dried soil powder was placed in a mixing tank, followed by the addition of tap water, stabilizer solution and SS in predetermined proportions. The components were thoroughly mixed under high-speed stirring to obtain homogeneous FSS.

2.4 Fluidity test

The test setup consisted of a hollow cylinder with an inner diameter of 80 mm and a height of 80 mm. The testing procedure was as follows: the cylinder was placed on a smooth glass plate, and the FSS was slowly poured into the cylinder until it was full. The cylinder was then lifted vertically at a constant speed, and the maximum slump flow diameter of the mixture was measured to determine its fluidity. The arithmetic mean of three test results was taken as the final fluidity value of the FSS.

2.5 Unconfined compressive strength (UCS)

In accordance with Chinese National Standards (GB/T 50123-2019), a uniform layer of mold release oil was applied to all interior surfaces of the 70.7 mm × 70.7 mm × 70.7 mm test mold. Subsequently, the flowable soil mixture was carefully introduced into the mold using a funnel, ensuring complete filling without air pockets. Subsequently, the mold was subjected to vibration compaction to ensure uniform density. The specimens were then hermetically sealed with plastic wrap and solidified for designated periods of 7, 14, and 28 days. Following dimensional measurements (length × width × thickness) using digital calipers, the specimens were mounted on a Shenzhen Suns UTM4304 Electronic Universal Testing Machine (China). Tests were conducted in displacement-controlled mode at a loading rate of 10 mm min^{-1} until specimen failure was achieved. The maximum compressive load was recorded, and the unconfined compressive strength (UCS) of the specimens was calculated using formula (1):

$$F_c = P/A \quad (1)$$

where F_c represents the unconfined compressive strength (MPa), P is the maximum load at failure (N) and A is the initial cross-sectional area of the specimen (mm^2).

2.6 Characterization

The viscosity of the stabilizer solution was analyzed using a Shanghai Nirun NDJ-88 digital viscometer (China). The functional groups of the stabilizer and soil stabilization product were analyzed using a Shimadzu FT-IR-8400 Fourier transform infrared (FT-IR) spectrometer (Japan). The molecular weight distribution of the stabilizer was analyzed using an Agilent 1260 Infinity II GPC system (USA) with an aqueous-phase mobile phase. The thermal properties of the stabilizer were analyzed using a Shanghai Techcomp DSC30 differential scanning calorimeter (China) (test range: −25 °C to 350 °C, heating rate: 5 °C min^{-1}). The N_2 adsorption–desorption isotherm of the soil stabilization product was determined using a Beijing PIODE SSA-4300 pore and specific surface area analyzer (China). The microstructure of the soil stabilization product was analyzed using a Zeiss EVO-08 scanning electron microscope (Germany).

The phase composition of the samples was analyzed using a Dandong Tongda TD3700 X-ray diffractometer (China) with the following parameters: voltage: 30 kV, current: 20 mA, scan rate: 0.1° s^{-1}, Scan range: 10°–70°.

3 Results and discussion

In this section, the characterization of the synthesized anionic polyelectrolytes is discussed in detail. The performance (fluidity, compressive strength) and structures of the soil matrix stabilized by as-prepared anionic polyelectrolytes and SS under different pH conditions were systematically researched. Additionally, the stabilization mechanism is discussed in detail.

3.1 Characterization of synthesized anionic polyelectrolytes

GPC analysis (Fig. 1a–c) revealed distinct molecular weight distributions. P(AA-*co*-AM) demonstrated moderate polydispersity (M_w = 37 924; range: 6768–379 020), L-PAA showed broad heterogeneity (M_w = 126 525; range: 241–7 022 968, spanning 4 orders), and H-PAA exhibited both high M_w > 192 571 and a relatively narrow distribution (24 299–7 829 662). The viscosities of P(AA-*co*-AM), H-PAA and L-PAA solutions were 200.8 Pa s, 164.8 Pa s and 102.8 Pa s, respectively (Fig. 1d). The highest viscosity of P(AA-*co*-AM) might be attributed to the strong entanglement within the copolymer chains.[23,24] The glass transition temperatures followed the order: P(AA-*co*-AM) (3.46 °C) > L-PAA (2.71 °C) > H-PAA (2.46 °C), suggesting increased chain restriction in the copolymer, further confirming the above hypothesis. Melting temperatures showed greater variation, with P(AA-*co*-AM) displaying significantly higher T_m (112.15 °C) compared to L-PAA (66.49 °C) and H-PAA (70.8 °C), correlating with their respective molecular architectures.

FT-IR was conducted to characterize the functional groups of the as-prepared stabilizers. As shown in Fig. 1f, a broad band located at 3606.2 cm^{-1} was assigned to –OH stretching vibrations. The peaks at 1731.7 cm^{-1}, 1405.3 cm^{-1} and 588.2 cm^{-1} corresponded to the stretching vibration of –C=O, in-plane bending vibration of –OH and deformation vibration of C–H, respectively. These characteristic peaks verified the molecular structural features of H-PAA. For L-PAA, the peak of the stretching vibration of –C=O and the in-plane bending vibration of –OH shifted to 1729.8 cm^{-1} and 1398.3 cm^{-1}, respectively, while the peak assigned to –OH became weaker. Compared to H-PAA, these differences suggested varied hydrogen-bonding networks in the low-M_w variant. For P(AA-*co*-AM), a new peak at 3118.3 cm^{-1} was attributed to primary amine symmetric stretching (–NH_2), while the peaks attributed to –COOH, –OH and C–C were all observed in the FT-IR spectrum of P(AA-*co*-AM), illustrating the successful incorporation of both AA and AM units in the copolymer structure.[25,26]

3.2 FSS stabilized by anionic polyelectrolyte

In this section, the performance, including fluidity and compressive strengths, and the structures of the soil matrix stabilized by the as-prepared anionic polyelectrolyte are investigated in detail.

3.2.1 Performance evaluation. The stabilized performance was assessed by preparing soil composites with 99% water content using engineering soil as the substrate. Three kinds of anionic polyelectrolytes [P(AA-*co*-AM), L-PAA, and H-PAA] were employed as stabilizers at various concentrations (1, 3, and 5 wt% relative to dry soil mass). As shown in Fig. 2a, when the dosages of P(AA-*co*-AM), L-PAA, and H-PAA were 1 wt%, the fluidities were 197.30 mm, 195.67 mm, and 202.33 mm, respectively (Fig. 2b), corresponding to excellent fluidity

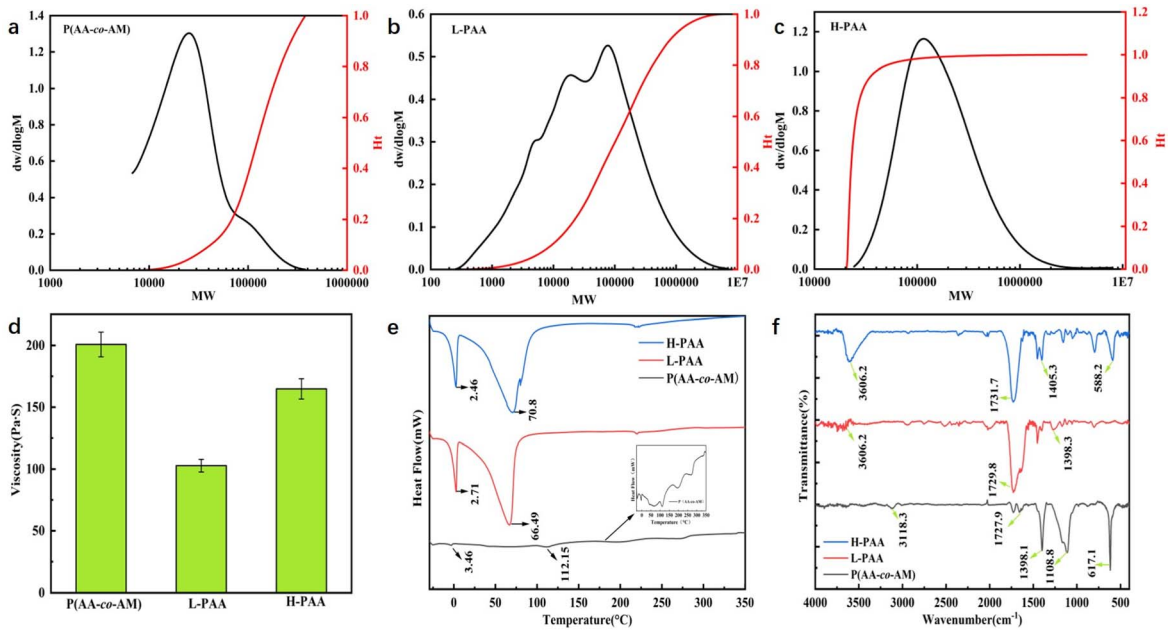

Fig. 1 GPC curves of (a) P(AA-*co*-AM), (b) L-PAA, and (c) H-PAA; (d) viscosity, (e) DSC curves and (f) FT-IR spectra of the as-prepared stabilizers.

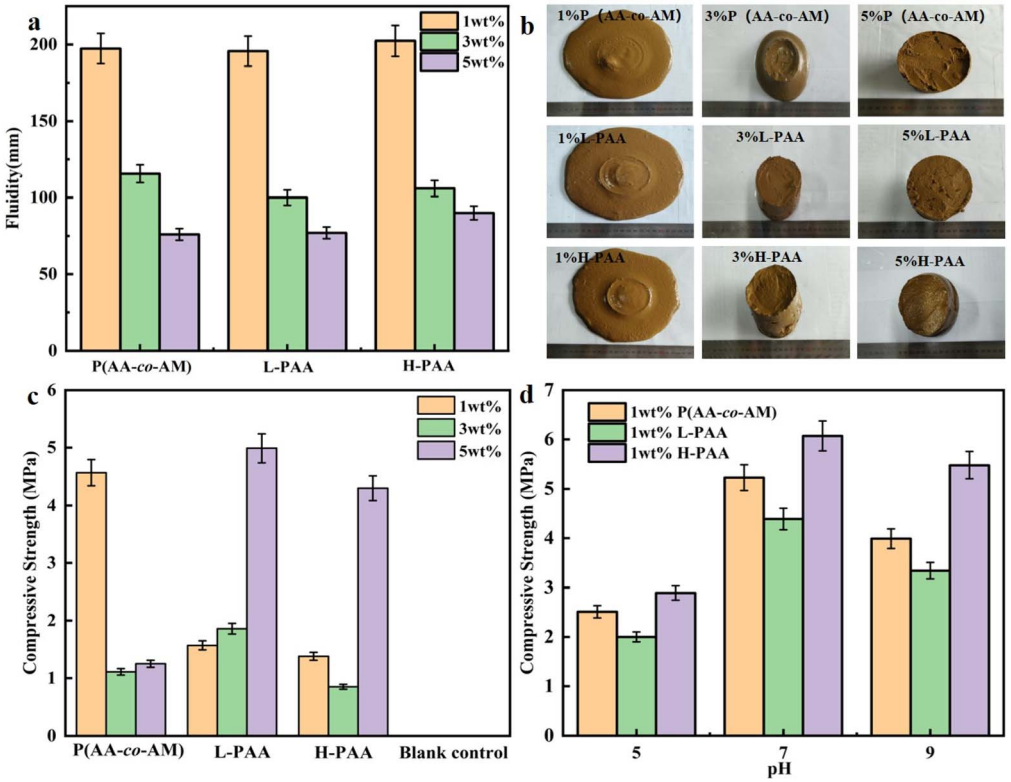

Fig. 2 (a) The fluidity and (b) corresponding digital photographs of FSS modified by P(AA-*co*-AM), L-PAA, and H-PAA with different contents; 28 day compressive strengths of soil mass stabilized by P(AA-*co*-AM), L-PAA, and H-PAA (c) with different contents (without tuning the pH value), and (d) at pH values of 5, 7, and 9.

satisfying the requirement for FSS (140–200 mm, and even >180 mm in critical engineering sections). The fluidity sharply reduced to 115.60 mm, 100.00 mm, and 106.00 mm for P(AA-*co*-AM), L-PAA, and H-PAA, respectively, when the dosages increased to 3 wt%. Upon further increasing the stabilizer content to 5 wt%, the FSS almost lost its fluidity, exhibiting decreases to 76.00 mm, 77.00 mm, and 90.00 mm, respectively. At this stage, the FSS transformed into a paste-like material and ceased to flow entirely, which was ascribed to the distinct hydration between hydrophilic polymer chains and free water within the system, leading to the enhancement of the interaction force (van der Waals force) between soil particles.[27,28]

As shown in Fig. 2c, the compressive strengths of cubic specimens obtained from FSS (stabilized with P(AA-*co*-AM) and maintained for 28 days under weather conditions) were 4.57 MPa, 1.11 MPa, and 1.25 MPa at additive concentrations of 1 wt%, 3 wt%, and 5 wt%, respectively. At 99% water content, elevated P(AA-*co*-AM) concentrations (≥3 wt%) were observed to compromise soil stabilization effectiveness. This strength reduction likely originated from preferential intermolecular interactions between polymer chains, which weakened their interaction with the soil-particle bonding. Additionally, the movement of polymer chains became more restricted when the soil mass was subjected to external forces, leading to reduced energy dissipation capacity and stress concentration, ultimately resulting in deteriorated mechanical performance.

The soil matrix stabilized by PAA series stabilizers exhibited a remarkable 28 day strength value of 4.99 MPa at most, which was much higher than that of the soil matrix stabilized by P(AA-*co*-AM). This phenomenon originated from the high-density crosslinking between $-COO^-$ on PAA chains and Ca^{2+} within the soil, establishing a rigid network. Moreover, the crosslinking also occurred between PAA chains and negative charge regions on soil particles, bridged by Ca^{2+}, further reinforcing the network.[29,30]

In summary, all three polyacrylate-based stabilizers [P(AA-*co*-AM), L-PAA, and H-PAA] effectively stabilized high-water-content (99%) soils, achieving satisfactory mechanical performance. Comprehensive evaluation of compressive strength and flowability characteristics revealed that a 1 wt% dosage represented the optimal formulation, meeting standard technical requirements for FSS (140–200 mm) fluidity. The anionic nature of these polyelectrolytes permits flexible selection based on specific project requirements. While higher dosages (3–5 wt%) produce stabilized soils with enhanced compressive strength (1.0–5.0 MPa), the concomitant reduction in fluidity may be advantageous for applications requiring rigid, low-mobility materials. This dosage-dependent behaviour enabled a tailored material designed for diverse construction scenarios.

The pH value of stabilizer solutions also governed the compressive strengths of the soil mass. As shown in Fig. 2d, the 28 day compressive strength of specimens modified by PAA or P(AA-*co*-AM) (1 wt%) in an acidic environment was much lower

than that in a neutral or basic environment, which can be ascribed to the protonation of $-COO^-$, weakening the ionic bridge interactions. However, most –COOH dissociated to $-COO^-$ at pH 9, while high contents of Na^+ would gather around PAA chains, resulting in electron screening effects reducing the ionic interactions between PAA chains and Ca^{2+} or soil particles, weakening the network.[31] Additionally, the soil matrix stabilized by H-PAA exhibited the best 28 day compressive strength of 6.07 MPa at pH 7. This is because at pH 7, the H-PAA chains were moderately extended, which would link multiple soil particles and Ca^{2+} to form a robust polymer bridge and 3D network. H-PAA exhibited superior stabilization performance compared to both L-PAA and P(AA-*co*-AM), particularly under neutral and alkaline conditions, benefiting from a large number of $-COO^-$ groups.[31]

3.2.2 Structure characterization. FT-IR was carried out to investigate the molecular structure of stabilized soil mass, which revealed the characteristic shifts in the asymmetric Si–O–Si stretching vibration (ν_{as}(Si–O–Si)) between sample groups (Fig. 3a). The untreated experimental soil exhibits a ν_{as}(Si–O–Si) absorption band at 1002 cm^{-1}, while hydration with tap water induced a blue shift to 1027 cm^{-1} in the tap water-stabilized soil sample. The ν_{as}(Si–O–Si) absorption peaks of the P(AA-*co*-AM)-stabilized sample, L-PAA-stabilized sample, and H-PAA-stabilized sample appeared at 1033 cm^{-1}, 1033 cm^{-1}, and 1099 cm^{-1}, respectively. It can be observed that the ν_{as}(Si–O–Si) absorption peaks of the polymer-stabilized samples shift to higher wavenumbers. The obvious shifts were induced by the reduction of the bond angle, which enhanced the coupling effect of the Si–O bond, increasing the vibrational energy level. These changes indicate that the double chain structure Q^3 and the network structure Q^4 in the polymer solidified body are higher than Q^0 in the isolated Si–O–Si or Si–O–Si monomer structures in the sand- and tap-water-solidified bodies.[24] These shifts provide direct spectroscopic evidence for polymer-induced silicate polycondensation.

Fig. 3b–e show the microstructure of soil mass stabilized by tap water and anionic polyelectrolytes. Compared to the soil mass stabilized by tap water, the obvious cementitious materials adhered to the surface of the soil mass (stabilized by anionic polyelectrolytes), binding individual soil particles together and reducing soil pores. The cementitious materials were randomly distributed within the microstructure of the soil, further enhancing the bonding force between particles in the stabilized soil.

The N_2 adsorption–desorption isotherm of 28 day polymer-stabilized soil mass (Fig. 3f) exhibited characteristic type IV(a) behavior with an H3-type hysteresis loop. The N_2 adsorption isotherm displayed a distinct plateau in the relative pressure range of 0.05–0.4 P/P_0, indicating the macroporous nature of the stabilized soil. An H3-type hysteresis loop was observed in the range of $0.4 < P/P_0 < 0.8$, indicative of multilayer adsorption and capillary condensation, revealing an irregular pore structure in the stabilized soil mass (the detailed parameters are shown in

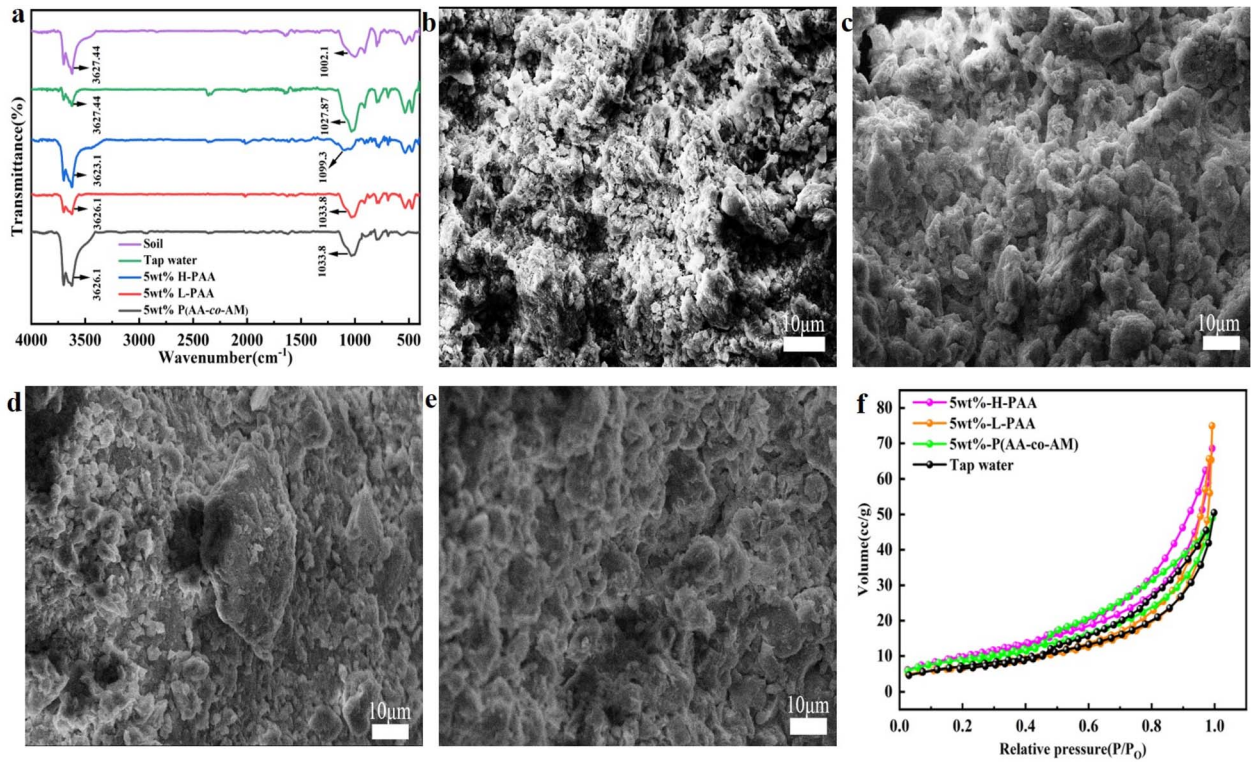

Fig. 3 (a) FT-IR spectra of original soil, stabilized soil mass with tap water, P(AA-*co*-AM), L-PAA, and H-PAA (5 wt%); SEM images of soil mass stabilized by (b) tap water, (c) P(AA-*co*-AM), (d) L-PAA, and (e) H-PAA; (f) N_2 adsorption–desorption isotherms of soil mass stabilized by tap water and as-synthesized anionic polyelectrolyte.

Table S2; BJH pore size distributions from the desorption branch are shown in Fig. S1). At $P/P_0 = 0.99$, the N_2 adsorption capacity was measured as 68.547 cm^3 for the tap water-stabilized sample, compared to 74.927 cm^3 (P(AA-*co*-AM)-stabilized), 33.045 cm^3 (L-PAA-stabilized), and 50.47 cm^3 (H-PAA-stabilized) soil mass. The tap water-stabilized sample showed a specific surface area of 37.628 $m^2\ g^{-1}$, with a single-point pore volume of 0.106591 cm^3 and an average pore radius of 56.7 Å. The P(AA-*co*-AM)-stabilized soil mass exhibited a specific surface area of 24.367 $m^2\ g^{-1}$, pore volume of 0.116506 cm^3, and average pore radius of 65.6 Å. For the L-PAA-stabilized soil, these values were 33.045 $m^2\ g^{-1}$, 0.076235 cm^3, and 46.1 Å, respectively, while the H-PAA-stabilized soil showed corresponding values of 26.379 $m^2\ g^{-1}$, 0.078482 cm^3, and 59.5 Å. Pore size distribution analysis revealed distinct differences between the samples: the tap water-stabilized sample contained pores predominantly in the 10–100 Å range with a higher fraction of larger pores, whereas the polymer-stabilized soil mass displayed a more concentrated distribution (10–50 Å) featuring a pronounced peak around 30 Å.

3.3 Dual-crosslinking stabilization system

In this section, the performance, including fluidity and compressive strengths, and the structures of the soil matrix stabilized by the as-prepared anionic polyelectrolyte cooperating with SS are investigated in detail.

3.3.1 Performance evaluation. To optimize the engineering performance of polymer-stabilized soil mass, a dual-crosslinking stabilization system was established by incorporating SS (as a complementary cementitious agent) into the anionic polyelectrolyte-FSS system. In this section, the SS contents were set at 1 wt%, 3 wt%, and 5 wt%, while the stabilizer concentration was fixed at 1 wt% with a water content of 99%. As shown in Fig. 4a, the fluidities of the FSS with 1 wt% SS addition were measured as 204.67 mm [P(AA-*co*-AM)], 246.33 mm (L-PAA), and 229.00 mm (H-PAA). However, upon increasing the SS content to 5 wt%, the fluidity of all the systems sharply decreased to 76.00 mm, not satisfying the requirement of construction engineering (Fig. 4b). It is known that SS can easily establish a brittle silica gel network ($SiO_2\ H_2O$), which enables the binding of water and soil particles. Additionally, the network crosslinked by polymer chains interpenetrated the silica gel network, establishing a double network system.[32–34] The establishment of the silica gel network was verified by the pure SS system, which showed a fluidity of 105.33 mm with an SS content of 5 wt%.

The compressive strengths of the dual-crosslinking systems are systematically researched in this section. The 7 day compressive strength of the soil matrix stabilized by 1 wt% SS and 1 wt% H-PAA was up to 2.02 MPa, while soil mass stabilized by a single component of SS at 1 wt% failed to achieve measurable solidification within 7 d (0 MPa) (Fig. 4c). Surprisingly, upon further increasing the dosage of SS to 3 wt% and 5 wt%, the 7 day compressive strengths decreased to 0.46 MPa and 0.96 MPa, respectively (Fig. 4c). It was demonstrated that the trace addition of SS (1 wt%) promoted the extension of the polymer chains to achieve the best bridging ability to establish a polymer-soil network, which interpenetrated the silica gel network to reinforce the structure. However, when the SS content was increased to 3 wt%, the large number of Na^+ species would strongly compress the double electric layer of the polymer chains, shielding the electrostatic repulsion between the chain segments, leading to the drastic curling and contraction of chains, transforming from a bridging conformation to an invalid coil conformation.[35,36] The curling chains lost the bridging ability with soil particles, damaging the polymer-soil network, generating poor compressive strength. Surprisingly, upon continuously increasing the SS content to 5 wt%, the compressive strength improved, illustrating that the silica gel network became a predominant structure, forming a continuous rigid framework that ran through the entire soil mass.[37,38] In contrast, the systems without SS exhibited poorer compressive strength, further confirming this concept (Fig. 4f).

Upon prolonging the curing time to 14 and 28 d, the soil matrix stabilized by 1 wt% SS exhibited the best compressive strengths of 3.25 MPa and 6.25 MPa, respectively, while they decreased with increasing SS content, which was consistent with the results of the 7 day compressive strengths (Fig. 4d and e). It was obvious that the dual-crosslinking systems displayed far better mechanical properties than those of the polymer-soil system, illustrating that the synergy of the inorganic–organic hybrid network greatly enhanced the mechanical properties of the soil matrix.

3.3.2 Structure characterization. The ν_{as}(Si–O–Si) absorption band appeared at 1024.01 cm^{-1} for the soil mass stabilized by single SS (1 wt%), while it shifted to 1029.08 cm^{-1}, 1043.03 cm^{-1} and 1033.65 cm^{-1} for dual-crosslinking soil masses stabilized by SS with contents of 1 wt%, 3 wt% and 5 wt% and H-PAA (1 wt%), respectively, confirming the enhanced Si–O bond coupling in the composite-stabilized systems compared to SS alone (Fig. 5a).

SEM images (Fig. 5b–d) demonstrated that the stabilized soil mass comprised polydisperse soil particles forming densely consolidated microstructures through multiple interfacial connection modes: point-to-point (discrete particle bonding), point-to-plane (particle-surface attachment), and plane-to-plane (sheet-like particle stacking). (Refer to Fig. S2 for SEM images of the control sample with only 1 wt% SS.)

XRD analysis (Fig. 5e) confirmed silica (SiO_2) as the predominant crystalline phase in all stabilized specimens. Notably, both SS and SS-polymer composite-stabilized samples demonstrated substantially attenuated diffraction peak intensities relative to the tap water-stabilized control. Although the polymer-soil particle interaction does not generate new crystalline phases, the –OH and $-NH_2$ groups on the polymer chains can bind with SiO_2 to form organic–inorganic hybrid structures, which can obscure the diffraction peaks of SiO_2 crystals. Meanwhile, SS generated amorphous silicic acid gel ($SiO_2 \cdot nH_2O$) in the stabilized bodies, which may also contribute to the attenuation of diffraction peak intensity.

BET analysis revealed that all stabilized soil masses (28 day) exhibited type IV nitrogen adsorption–desorption isotherms. The presence of a gentle plateau in the $0.05 < P/P_0 < 0.4$ range

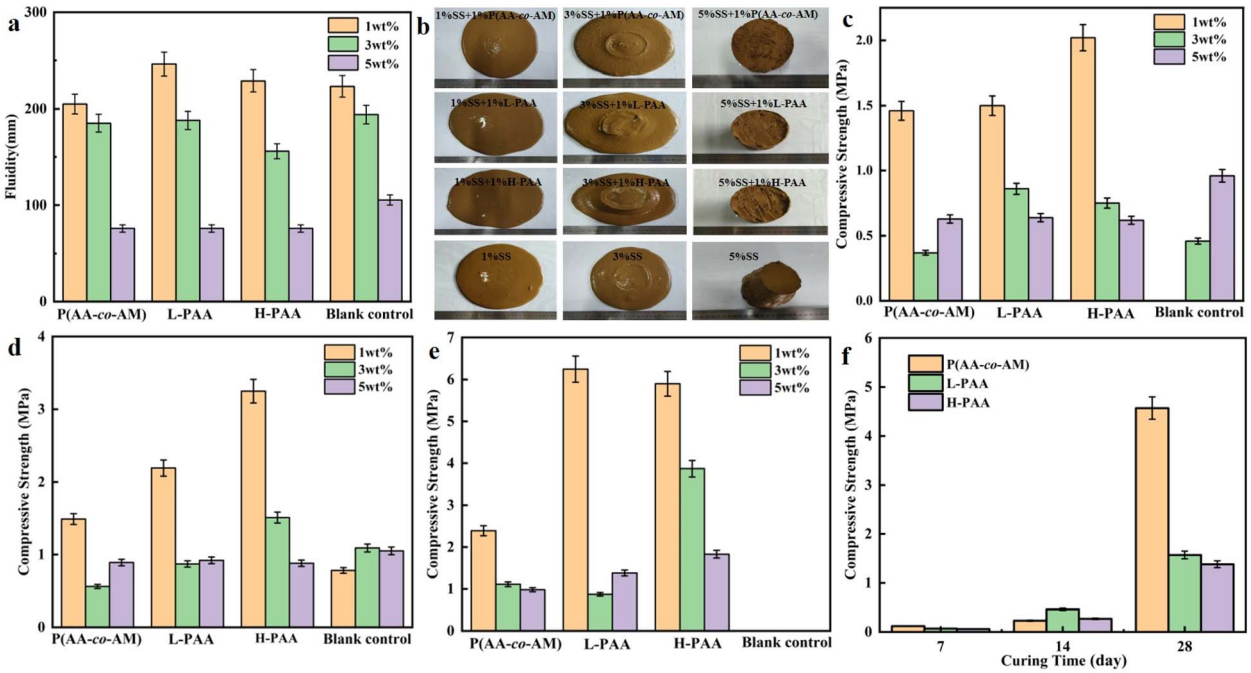

Fig. 4 (a) The fluidity and (b) corresponding digital photographs of FSS reinforced by SS with different contents; compressive strengths of (c) 7 day, (d) 14 day, and (e) 28 day stabilized specimens with SS and anionic polyelectrolytes (1 wt%); (f) compressive strengths of 7, 14, and 28 day stabilized specimens with 1 wt% anionic polyelectrolyte (no SS).

confirmed their macroporous nature, while the H3-type hysteresis loop observed at $0.4 < P/P_0 < 0.8$ indicated multilayer adsorption and capillary condensation within irregular pore structures (Table S3, Fig. S3). The BET surface area of the soil mass stabilized by 1 wt% SS and 1 wt% H-PAA was 13.584 $m^2 g^{-1}$ with an average pore radius of 141.7 Å. When the content of SS was increased to 3 wt% and 5 wt%, the BET surface area improved to 17.156 $m^2 g^{-1}$ and 18.663 $m^2 g^{-1}$, respectively, and the average pore radius reduced to 131.9 Å and 63.9 Å, respectively. In contrast, the soil mass stabilized by SS (1 wt%)

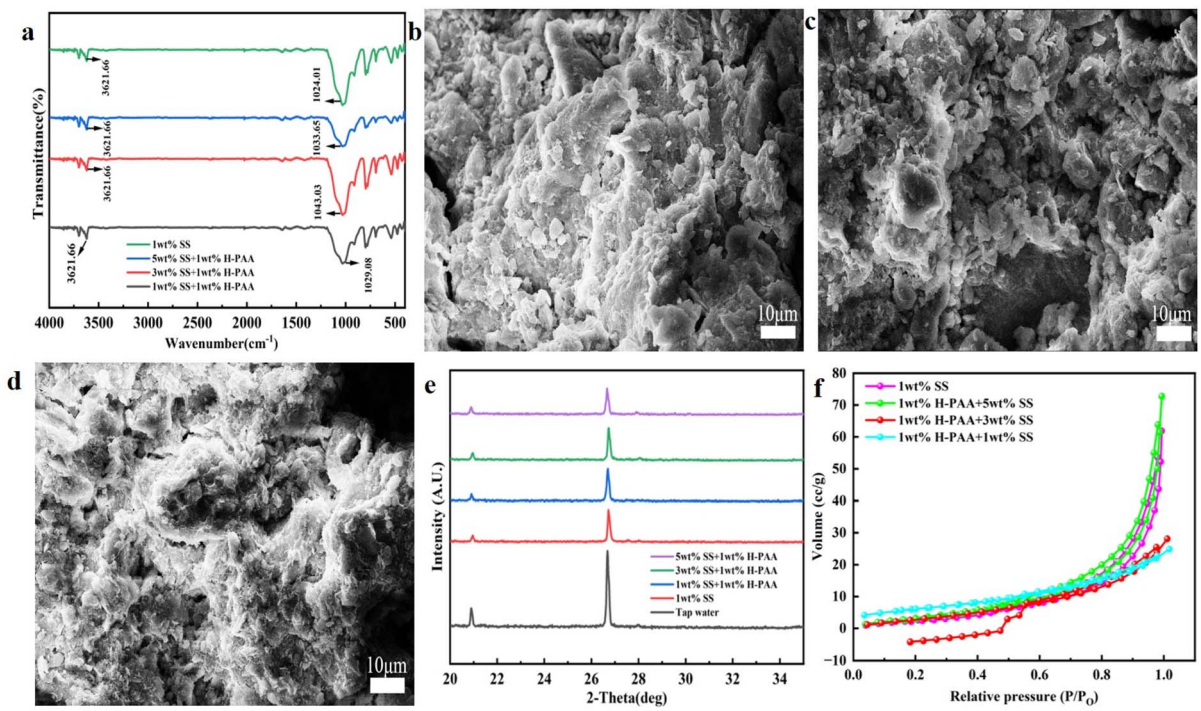

Fig. 5 (a) FT-IR spectra of soil mass stabilized by SS and H-PAA with different contents; SEM images of soil mass stabilized by H-PAA (1 wt%) and (b) 1 wt%, (c) 3 wt% and (d) 5 wt% SS; (e) XRD and (f) BET analysis of soil mass stabilized by H-PAA (1 wt%) and SS with different contents.

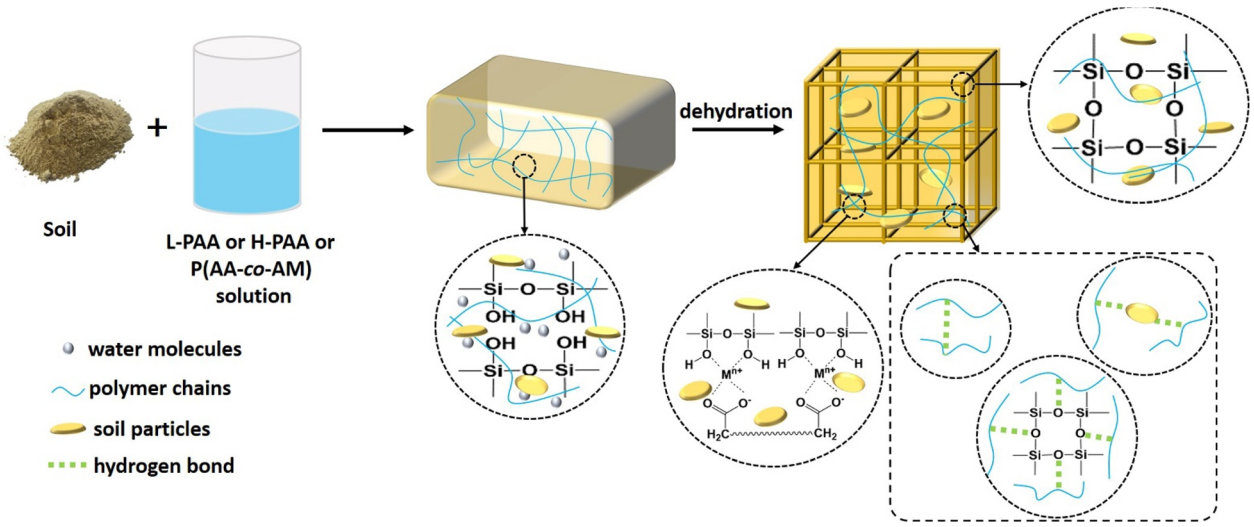

Scheme 2 The stabilization mechanism for soil mass with anionic polyelectrolytes [P(AA-*co*-AM), L-PAA and H-PAA].

exhibited a larger BET surface area (22.548 $m^2 g^{-1}$) and smaller average pore radius (34.3 Å).

In summary, SS incorporation filled the pores within the soil mass to reduce porosity, improving interparticle bonding and structural stability through densifying its backbones. The synergistic interaction between the polymeric network and SS further optimized the mechanical performance of the soil mass.

3.4 Stabilization mechanism

The copolymers [P(AA-*co*-AM)] and PAA synthesized in this project were high-molecular-weight linear polymers capable of forming interpenetrating polymeric networks within the soil matrix. Notably, the sandy soil used in this experiment primarily consists of SiO_2 with minor silicate mineral components. The synthesized copolymers [P(AA-*co*-AM)] and PAA contained highly hydrophilic –COOH and $–NH_2$ functional groups, endowing them with exceptional hydrophilicity. These polymers underwent dehydration-condensation reactions with surface –OH groups on different siloxane chains, resulting in crosslinking and subsequent soil solidification. Furthermore, the –COOH groups on P(AA-*co*-AM) and PAA chelated with cations (*e.g.* Ca^{2+}, Fe^{3+}, and Mg^{2+}) present in clay minerals, while simultaneously forming hydrogen bonds with silicate surface –OH groups. This dual interaction mechanism facilitated the establishment of stable macromolecular network structures between soil particles, ultimately achieving effective soil stabilization (Scheme 2).

In the stabilization procedure, SS reacted with water to generate silicic acid (H_4SiO_4) and NaOH. During the dehydration, the silicic acid underwent further polycondensation to

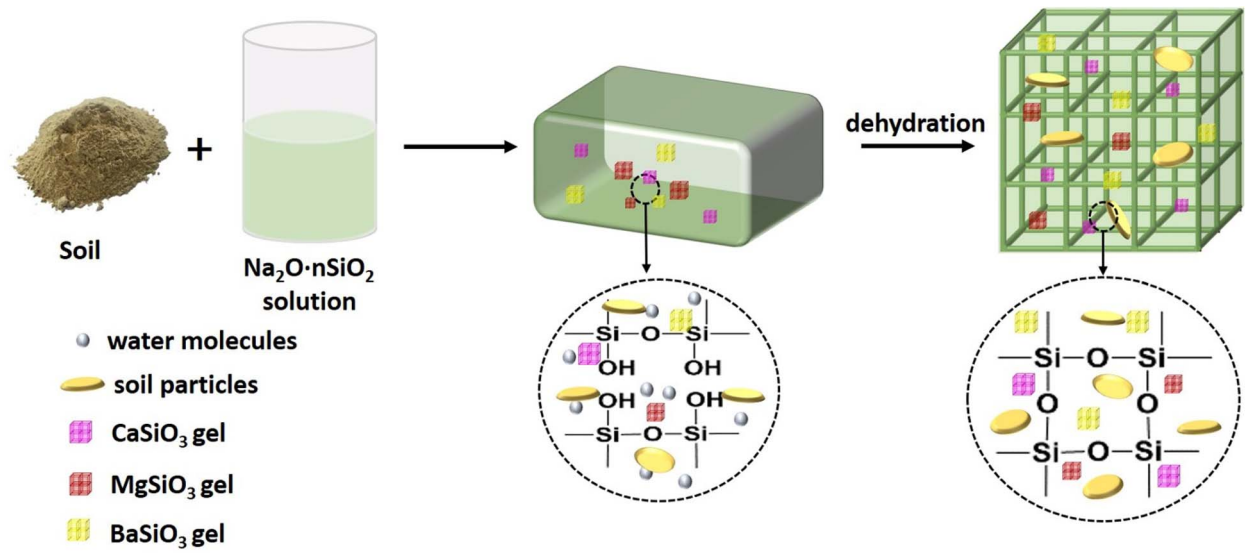

Scheme 3 The stabilization mechanism of soil mass with sodium silicate (SS).

form a three-dimensional network-structured silica gel ($SiO_2 \cdot nH_2O$). Ultimately, the silica gel continuously dehydrated and solidified, resulting in the formation of a rigid siloxane (Si–O–Si) framework, thereby enhancing the mechanical strength of the soil mass. Furthermore, the silica gel structure firmly bound soil particles through physical adsorption and chemical bonding (*e.g.* reactions with surface –OH groups on soil particles), thereby advancing the compactness and compressive strength of the overall structure.[25,26] Additionally, the nano-scale silica gel particles generated during the stabilization process filled micropores or microcracks within the matrix, reducing soil defects and improving densification (Scheme 3).

In the dual-crosslinking system, the incorporation of SS along with P(AA-*co*-AM) and PAA induced a synergistic effect between the silicate and polymeric components. This interaction significantly accelerated the stabilization rate while simultaneously endowing the soil matrix with enhanced compressive strength (Scheme 1).

4 Conclusions

In summary, in this work, a series of polyelectrolyte-based stabilizers was synthesized, cooperating with SS to construct hybrid FSS systems, which exhibited excellent fluidity (>200 mm), satisfying construction requirements. After curing for 28 days, the 28 day compressive strength of the soil matrix reached 6.25 MPa. Characterization technologies (FT-IR, SEM, BET, and XRD) were employed to investigate the stabilization mechanism. This work overcame the intrinsic weakness of single cementitious and organic systems, combining their advantages to achieve the cyclic utilization of engineering surplus soils, which is important in the field of construction engineering.

Author contributions

Conceptualization: Dengliang He and Shishan Xue; investigation: Haiyang Zhang, Yi Liu; writing—original draft preparation: Haiyang Zhang; writing—review and editing: Haiyang Zhang, Dengliang He, Shishan Xue; project administration: Dengliang He, Shishan Xue; funding acquisition: Dengliang He, Shishan Xue, Shuxin Liu, Mengyong Ran.

Conflicts of interest

There are no conflicts to declare.

Data availability

The data supporting this article are available from the corresponding author upon reasonable request.

Additional data supporting this article have been included as part of the supplementary information (SI). Supplementary information: experimental parameters, BET parameters and SEM image. See DOI: https://doi.org/10.1039/d5ra04933d.

Acknowledgements

This work was financially supported by Open Fund of Vanadium and Titanium Resource Comprehensive Utilization Key Laboratory of Sichuan Province (2023FTSZ02), Mianyang Teachers' College Start-up Funding (QD2021A11) and Innovation Team of Mianyang Teachers' College (CXTD2023PY06).

Notes and references

1 R. Wang, C. S. Tang, X. H. Pan, D. L. Wang, Z. H. Dong, X. Y. Zhang and X. C. Lu, *J. Rock Mech. Geotech. Eng.*, 2024, **16**, 3760.
2 M. F. Noaman, M. Haq, M. A. Khan, K. Ali and H. Kamy, *Case Stud. Constr. Mater.*, 2024, **21**, e03628.
3 M. Haq, M. A. Khan, S. Ali, K. Ali, M. Yusuf, H. Kamyab and K. Irshad, *Environ. Res.*, 2024, **256**, 119217.
4 W. J. Hou, J. Wang, D. L. Feng, S. H. Liang, F. Liu and S. J. Wu, *KSCE J. Civ. Eng.*, 2024, **29**, 100125.
5 A. M. Abdelbaset, D. Katunský, M. Zeleňáková and M. H. El-Feky, *Case Stud. Constr. Mater.*, 2024, **21**, e03662.
6 P. Eshghi, M. Azadi and H. Ahmadi, *Results Eng.*, 2024, **4**, 103529.
7 Z. Y. Xie, D. Yu and J. Wang, *Case Stud. Constr. Mater.*, 2025, **22**, e04204.
8 Y. C. Luan, X. J. Ma, Y. Ma, X. Y. Liu, S. Q. Jiang and J. M. Zhang, *Case Stud. Constr. Mat.*, 2023, **19**, e02397.
9 L. Wang, Y. S. Yao and J. Li, *Case Stud. Constr. Mat.*, 2024, **21**, e04075.
10 M. L. Liu, M. Saberian, J. Li, J. S. Zhu, R. Roychand and C. Q. Li, *Case Stud. Constr. Mater.*, 2025, **22**, e04256.
11 M. Ayeldeen, A. Negm, M. El-Sawwaf and M. Kitazume, *J. Rock Mech. Geotech.*, 2017, **9**, 329.
12 Q. Z. Tian, Y. C. Bai, Y. H. Pan, C. S. Chen, S. Yao, K. Sasaki and H. J. Zhang, *Molecules*, 2022, **27**, 4570.
13 F. Ayub and S. A. Khan, *Constr. Build. Mater.*, 2023, **404**, 133195.
14 J. F. Young, *Cem. Concr. Res.*, 1972, **2**, 415.
15 S. Yavari, H. Kamyab, T. S. B. A. Manan, S. Chelliapan, R. Asadpour, S. Yavari, N. B. Sapari, L. Baloo, A. B. C. Sidik and I. Kirpichnikova, *Chemosphere*, 2022, **303**, 134957.
16 C. C. Shen, S. Petit, C. J. Li, C. S. Li, N. Khatoon and C. H. Zhou, *Appl. Clay Sci.*, 2020, **198**, 105778.
17 S. Weiss, D. Hirsemann, B. Biersack, M. Ziadeh, A. H. E. Müller and J. Breu, *Polymer*, 2013, **54**, 1388.
18 A. Soltani, A. Deng, A. Taheri and B. C. O'Kelly, *J. Rock Mech. Geotech.*, 2022, **14**, 252.
19 S. A. M. Moayed, M. Arabani and H. Ahmadi, *Results Eng.*, 2025, **26**, 105318.
20 M. S. Baghini, A. Ismail, M. P. Asghar and G. M. Fendereski Sadeghi, *Int. J. Pavement Res. Technol.*, 2018, **11**, 458.
21 A. Jarjusey, K. Hayano, A. A. Kassa, S. Raihan and Y. Mochizuki, *Results Eng.*, 2024, **24**, 103166.
22 S. Q. Wang, X. X. He, G. H. Cai, J. S. Li, H. J. Qin, Y. Y. Ma, S. M. Gong and L. Lang, *Dev. Built Environ.*, 2024, **17**, 100323.
23 M. Tally and Y. Atassi, *Polym. Bull.*, 2016, **73**, 3183.

24 H. Kamyab, S. Chelliapan, E. Khalili, S. Rezania, B. Balasubramanian, M. M. Taheri, D. S. Racines, S. Rajendran and M. Yusuf, *J. Hazard. Mater. Adv.*, 2025, **18**, 100673.
25 F. M. A. Noa and A. Jacobs, *J. Mol. Struct.*, 2017, **1139**, 60.
26 M. Alizadeh, S. Abdi, S. M. Abdoli, H. Hazrati and M. Salami-Kalajahi, *Int. J. Chem. Eng.*, 2024, 6346033.
27 Z. M. He, A. Shen, Y. C. Guo, Z. H. Lyu, D. S. Li, X. Qin, M. Zhao and Z. L. Wang, *Constr. Build. Mater.*, 2019, **225**, 569.
28 D. L. Bouranis, A. G. Theodoropoulos and J. B. Drossopoulos, *Commun. Soil Sci. Plant Anal.*, 1995, **26**, 1455.
29 W. Huang, X. Y. Geng, Z. Liu and C. Y. Zhou, *Chem. Phys. Lett.*, 2022, **806**, 139985.
30 Y. C. Luan, X. J. Ma, Y. Ma, X. Y. Liu, S. Q. Jiang and J. M. Zhang, *Case Stud. Constr. Mater.*, 2023, **19**, e02397.
31 A. T. S. Azhar, M. I. S. Fazlina, Z. M. Nizam, Y. M. Fairus, M. N. A. Hakimi, Y. Riduan and P. Faizal, *IOP Conf. Ser.:Mater. Sci. Eng.*, 2017, **226**, 012063.
32 N. Latifi, S. Horpibulsuk, C. L. Meehan, M. Z. A. Majid, M. M. Tahir and E. T. Mohamad, *J. Mater. Civ. Eng.*, 2016, **29**, 04016204.
33 K. Zhang, M. Y. Jing, H. F. Lu, H. Dai, Z. Y. Li, X. X. Kong and P. H. Deng, *Environ. Res.*, 2025, **281**, 121999.
34 A. K. Srivastava, D. Iyer, M. Galadari, S. Srivastava and A. Singh, *Polym. Compos.*, 2025, **46**, 11203.
35 T. Zhao, N. Feng, Y. H. Zhao and G. L. Zhang, *Colloids Surf., A*, 2020, **606**, 125482.
36 A. Pal and S. Yadav, *J. Mol. Liq.*, 2017, **241**, 584.
37 Y. Shao, Y. T. Wang, F. Yang, C. G. Du, J. W. Zhu, Y. Ran, Q. C. Bao, Y. Y. Shan and W. G. Zhang, *Molecules*, 2024, **29**, 1472.
38 Y. P. Cao, H. Lin, T. Zong, X. B. Xu, M. D. Li, X. Bian and Z. Q. Li, *Sci. Rep.*, 2024, **14**, 31947.